Sensorless Control of AC Motor - Where are we now?

Sungmin Kim, and Seung-Ki Sul
Seoul national university Power Electronics Center (SPEC)
Seoul National University
E-mail: sulsk@plaza.snu.ac.kr

Abstract — In the AC machine drives, the rotor position information is the crucial information for high performance drive system. There have been more than 30 years of researches to get the rotor position information without explicit position sensors such as encoders and resolvers. Some research results are commercialized and applied to industrial field. However, still the performance of sensorless drive is limited. In this paper, the overview of the sensorless drive techniques, especially regarding Interior Permanent Magnet Synchronous Machine (IPMSM), are described. Some research topics for future study are suggested.

I. INTRODUCTION

After the idea of vector control of AC machine drive brought out, the information of the rotor flux linkage is crucial information for the control of the torque of AC machine [1]. The rotor position is commonly obtained by explicit sensors: encoder, resolver, hall sensor, and etc. However, these mechanical rotor position sensors lead to some undesirable effects in the system design: additional cost and volume, noise problems, and related reliability issues. To overcome these problems, the position sensorless drive techniques of AC machine has been studied for over last three decades [2]-[3], and some of them are commercialized and applied to industrial fields. However, still, the performance of the sensorless drive is limited. Some commercialized techniques had shown reasonable performances in overall operating conditions except low speed/low frequency region. For last ten years, sensorless drive techniques based on high frequency signal injection methods have evolved. Those techniques can guarantee the reasonable torque control performance even at zero speed/zero frequency. At early stage of the high frequency injection sensorless drive, the speed control bandwidth is limited to less than 10Hz. Until recently, many ideas to enhance the bandwidth of the sensorless control using signal injection have been reported. In this paper, some key ideas of the sensorless control for Interior Permanent Magnet Machine are reviewed and there operation principles are described.

While the conventional current control with position sensor uses the real-time rotor position in reference frame transformation as in Fig. 1(a), the sensorless current control uses the estimated rotor position which is obtained by measured or estimated voltages and current information as in Fig. 1(b). The voltage can be directly measured. But, because of the cost and noise issues, as shown in Fig. 1(b), the reference voltage to AC machine is usually used as the voltage information in the most case of the sensorless drive system.

The sensorless methods of AC machine drives can be generally classified to two groups according to the principle of the rotor position estimation. Sensorless methods in the first group use the back EMF, and the methods in the second group rely on the magnetic saliency of the rotor caused by the rotor structure itself or by the injected signal. In the first group, to extract the rotor position information from the back EMF, it uses the electric model of the AC machine in the stationary frame or the estimated rotor reference frame. It presents good performance in the medium and high speed operating region of AC machine. And it is

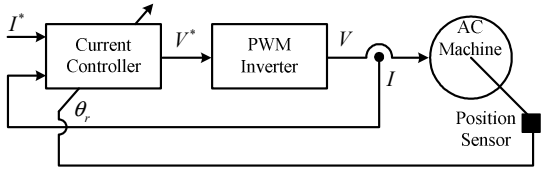

(a) Current control structure with a position sensor

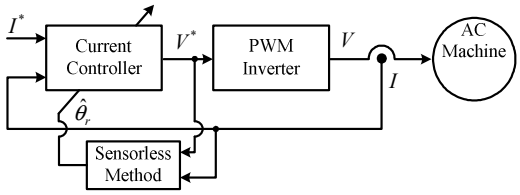

(b) Current control structure by the sensorless method

Fig. 1. Current control structures with sensed position and with estimated position.

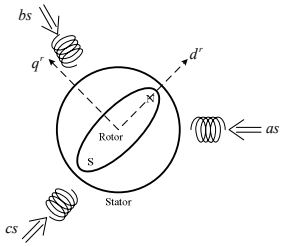

Fig. 2. Model of Interior Permanent Magnet Synchronous Machine.

commercialized by many companies. The performance of the commercial products is quite satisfactory for the most of low end drive application above 5% of the rated speed with rated load in motoring operation. The bandwidth of the speed regulation loop can be extended more than 10Hz. However, at standstill or very low rotating speed, because the voltage from the back EMF is proportional to the rotating speed, the signal is too weak to be used as the position information and the signal is easily contaminated by the measurement noises or the nonlinear effects of PWM inverter. In the second group, rotor position is estimated from the inherent characteristics of AC machine, the magnetic saliency. The magnetic saliency causes the spatial inductance distribution according to the rotor position. The saliency comes from the structure of the rotor itself or from the secondary effects by the injected signal itself. The signal can be injected as current or voltage to the machine. Because of the limited current regulation bandwidth of the most AC drive, the voltage signal injection technique is usually employed. Regardless of the hard works from many researchers in the world, the performance of sensorless drive of the induction machine for general purpose at zero frequency is still awkward. The reason may not be from the control technique itself but from the diversity of the induction machine itself. Still, a control technique cannot adapt to all various types of induction machines.

Hence, in this paper the research results on the sensorless operation of AC machine, especially, Interior Permanent Magnet Synchronous Machine (IPMSM) for last 20 years are described. The general purpose sensorless drive system of IPMSM based on high frequency signal injection method had been commercialized

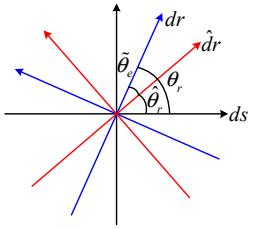

Fig. 3. Stationary frame, rotor reference frame, and estimated rotor reference frame in d-q reference plane.

and its performance has been proved in the field for last three years [4]. The basic principles of both of the back EMF based sensorless methods and the magnetic saliency based sensorless methods are derived and implementation techniques are described in this paper.

II. Back EMF Based Sensorless Control

A. Fundamental Principle

In Fig. 2 an analytical model of an IPMSM is shown. Here, d-axis is placed on the magnetic axis of the rotor and q-axis is perpendicular to d-axis in the rotational direction. The voltage equation based on d-q axis is given (1) where $v_{ds}^{\ r}$, $v_{qs}^{\ r}$ is voltage references, $i_{ds}^{\ r}$, $i_{qs}^{\ r}$ is measured currents, R_S is the stator resistance, λ_f is the flux linkage of the permanent magnet, and L_{ds}, L_{qs} are d-q axis inductance, respectively.

$$\begin{aligned} v_{ds}^{r} &= R_s i_{ds}^{r} + L_{ds}\frac{di_{ds}^{r}}{dt} - \omega_r L_{qs} i_{qs}^{r} \\ v_{qs}^{r} &= R_s i_{qs}^{r} + L_{qs}\frac{di_{qs}^{r}}{dt} + \omega_r L_{ds} i_{ds}^{r} + \omega_r \lambda_f \end{aligned} \quad . \tag{1}$$

The induced voltage by the rotating permanent magnet flux linkage is placed on the q-axis of rotor reference frame. That leads to us to estimate the rotor position. To analyze the sensorless methods, the reference frames have to be defined as shown in Fig. 3. When the real rotor position is θ_r, the position error, $\tilde{\theta}_r$, between the real rotor position and the estimated position, $\hat{\theta}_r$ can be presented as (2).

$$\tilde{\theta}_r = \theta_r - \hat{\theta}_r \quad . \tag{2}$$

Because the operating reference frame is the estimated rotor reference frame, the voltage equation in (1) should be transformed by position error, $\tilde{\theta}_r$ as (3). Then, the voltage equation can be described as (4) in the estimated rotor reference frame.

$$v_{dqs}^{\hat{r}} = T_{\tilde{\theta}_r}^{-1} v_{dqs}^{r} \qquad i_{dqs}^{\hat{r}} = T_{\tilde{\theta}_r}^{-1} i_{dqs}^{r} \quad . \tag{3}$$

$$v_{dqs}^{\hat{r}} = \begin{bmatrix} v_{ds}^{\hat{r}} \\ v_{qs}^{\hat{r}} \end{bmatrix} = R_s \begin{bmatrix} i_{ds}^{\hat{r}} \\ i_{qs}^{\hat{r}} \end{bmatrix} + L_a \frac{d}{dt}\begin{bmatrix} i_{ds}^{\hat{r}} \\ i_{qs}^{\hat{r}} \end{bmatrix} + \begin{bmatrix} e_{ds}^{\hat{r}} \\ e_{qs}^{\hat{r}} \end{bmatrix} \quad . \tag{4}$$

$$\begin{bmatrix} e_{ds}^{\hat{r}} \\ e_{qs}^{\hat{r}} \end{bmatrix} = \tilde{\omega}_r L_b \begin{bmatrix} i_{ds}^{\hat{r}} \\ i_{qs}^{\hat{r}} \end{bmatrix} + \omega_r L_c \begin{bmatrix} i_{ds}^{\hat{r}} \\ i_{qs}^{\hat{r}} \end{bmatrix} + \omega_r \lambda_f \begin{bmatrix} -\sin\tilde{\theta}_r \\ \cos\tilde{\theta}_r \end{bmatrix} \quad . \tag{5}$$

$$L_a = \begin{bmatrix} L_{ds}\cos^2\tilde{\theta}_r + L_{qs}\sin^2\tilde{\theta}_r & (L_{ds}-L_{qs})\sin\tilde{\theta}_r\cos\tilde{\theta}_r \\ (L_{ds}-L_{qs})\sin\tilde{\theta}_r\cos\tilde{\theta}_r & L_{ds}\sin^2\tilde{\theta}_r + L_{qs}\cos^2\tilde{\theta}_r \end{bmatrix} \quad . \tag{6}$$

$$L_b = \begin{bmatrix} (-L_{ds}+L_{qs})\sin\tilde{\theta}_r\cos\tilde{\theta}_r & L_{ds}\cos^2\tilde{\theta}_r + L_{qs}\sin^2\tilde{\theta}_r \\ -L_{ds}\sin^2\tilde{\theta}_r - L_{qs}\cos^2\tilde{\theta}_r & (L_{ds}-L_{qs})\sin\tilde{\theta}_r\cos\tilde{\theta}_r \end{bmatrix} \quad . \tag{7}$$

$$L_c = \begin{bmatrix} (-L_{ds}+L_{qs})\sin\tilde{\theta}_r\cos\tilde{\theta}_r & -L_{ds}\sin^2\tilde{\theta}_r - L_{qs}\cos^2\tilde{\theta}_r \\ L_{ds}\cos^2\tilde{\theta}_r + L_{qs}\sin^2\tilde{\theta}_r & (L_{ds}-L_{qs})\sin\tilde{\theta}_r\cos\tilde{\theta}_r \end{bmatrix} \quad . \tag{8}$$

Assuming the estimated speed is synchronized with the real speed ($\omega_r \approx \hat{\omega}_r$) even though the position error, $\tilde{\theta}_r$ exists, the effective EMF voltage can be described as (9).

$$\begin{bmatrix} e_{ds}^{\hat{r}} \\ e_{qs}^{\hat{r}} \end{bmatrix} \approx \omega_r \left(L_{qs} - L_{ds}\right) \begin{bmatrix} i_{ds}^{\hat{r}}\tilde{\theta}_r \\ -i_{qs}^{\hat{r}}\tilde{\theta}_r \end{bmatrix} + \begin{bmatrix} -L_{qs} i_{qs}^{\hat{r}} - \lambda_f \tilde{\theta}_r \\ L_{ds} i_{ds}^{\hat{r}} + \lambda_f \end{bmatrix} \tag{9}$$

where $\omega_r \approx \hat{\omega}_r$, $\cos\tilde{\theta}_r \approx 1$, $\sin\tilde{\theta}_r \approx \tilde{\theta}_r$, $\tilde{\theta}_r >> \tilde{\theta}_r^{\,2}$. Then the position error can be derived from the effective EMF voltage as (10).

$$\begin{bmatrix} e_{ds}^{\hat{r}} \\ e_{qs}^{\hat{r}} \end{bmatrix} - \begin{bmatrix} -L_{qs} i_{qs}^{\hat{r}} \\ L_{ds} i_{ds}^{\hat{r}} + \lambda_f \end{bmatrix} \approx \omega_r \begin{bmatrix} \left(L_{qs} - L_{ds}\right) i_{ds}^{\hat{r}} - \lambda_f \\ -\left(L_{qs} - L_{ds}\right) i_{qs}^{\hat{r}} \end{bmatrix} \tilde{\theta}_r \quad . \tag{10}$$

From (10), the rotor position error can be obtained and it is used an input to a state filter or an observer to estimate the rotor position and speed.

These back EMF based sensorless methods estimate the rotor position and speed from the stator voltages and currents. With this basic idea, many different implementation methods have been reported. Some methods are based on the estimation of the back EMF voltage from the permanent magnet flux linkage using a state observer or a Kalman filter. Another methods use the voltage or current error between the measured values and the calculated values at the estimated rotor position. Others use the fundamental stator voltage to minimize the rotor position error.

B. Back EMF Estimation based Sensorless Methods

Sensorless control methods based on the back EMF estimation extract the back EMF voltage from (11) which is simplified from (4) and (5).

$$\begin{aligned} v_{ds}^{\hat{r}} &= R_s i_{ds}^{\hat{r}} + L_{ds}\frac{di_{ds}^{\hat{r}}}{dt} - \hat{\omega}_r L_{qs} i_{qs}^{\hat{r}} - \hat{\omega}_r \lambda_f \sin\tilde{\theta}_r \\ v_{qs}^{\hat{r}} &= R_s i_{qs}^{\hat{r}} + L_{qs}\frac{di_{qs}^{\hat{r}}}{dt} + \hat{\omega}_r L_{ds} i_{ds}^{\hat{r}} + \hat{\omega}_r \lambda_f \cos\tilde{\theta}_r \end{aligned} \quad . \tag{11}$$

There are two kinds of approaches to estimate the back EMF voltage. One method is calculating the back EMF voltage from (11) directly. Under the assumption of the electrical steady-state, the back EMF voltage can be estimated with following simple calculation.

$$\begin{aligned} -\hat{\omega}_r \lambda_f \sin\tilde{\theta}_r &\approx v_{ds}^{\hat{r}} - R_s i_{ds}^{\hat{r}} + \hat{\omega}_r L_{qs} i_{qs}^{\hat{r}} \\ \hat{\omega}_r \lambda_f \cos\tilde{\theta}_r &\approx v_{qs}^{\hat{r}} - R_s i_{qs}^{\hat{r}} - \hat{\omega}_r L_{ds} i_{ds}^{\hat{r}} \end{aligned} \quad . \tag{12}$$

If the machine parameters are correct, the position error is derived as (13).

$$\tilde{\theta}_r = \tan^{-1}\left(\frac{\hat{\omega}_r \lambda_f \sin\tilde{\theta}_r}{\hat{\omega}_r \lambda_f \cos\tilde{\theta}_r}\right) \quad . \tag{13}$$

Because of the assumption of the electrical steady state ignoring the variation of current, this direct calculation is not suitable to estimate the position error when the current varies rapidly according to the load torque disturbance or torque reference change.

The other method is using the state observer [5]. From (11), the state equations can be derived and the closed loop state observer would be implemented as (14) and (15) under the assumption that the back EMF variation is negligible.

$$\begin{aligned} \dot{\hat{x}} &= A\hat{x} + Bu + L\left(y - c\hat{x}\right) \\ &= \begin{bmatrix} -\frac{R_s}{L_{ds}} & \frac{\hat{\omega}_r L_{qs}}{L_{ds}} & \frac{1}{L_{ds}} & 0 \\ \frac{-\hat{\omega}_r L_{ds}}{L_{qs}} & -\frac{R_s}{L_{qs}} & 0 & \frac{1}{L_{qs}} \\ 0 & 0 & 0 & 0 \\ 0 & 0 & 0 & 0 \end{bmatrix} \begin{bmatrix} \hat{i}_{ds}^{\hat{r}} \\ \hat{i}_{qs}^{\hat{r}} \\ \hat{e}_{ds}^{\hat{r}} \\ \hat{e}_{qs}^{\hat{r}} \end{bmatrix} + \begin{bmatrix} \frac{1}{L_{ds}} & 0 \\ 0 & \frac{1}{L_{qs}} \\ 0 & 0 \\ 0 & 0 \end{bmatrix} \begin{bmatrix} v_{ds}^{\hat{r}} \\ v_{qs}^{\hat{r}} \end{bmatrix} + L\left(y - \hat{y}\right) \end{aligned} \quad . \tag{14}$$

$$\hat{y} = \begin{bmatrix} \hat{i}_{ds}^{\hat{r}} \\ \hat{i}_{qs}^{\hat{r}} \end{bmatrix} = \begin{bmatrix} 1 & 0 & 0 & 0 \\ 0 & 1 & 0 & 0 \end{bmatrix} \hat{x} = C\hat{x} \quad . \tag{15}$$

Then, the position error can be obtained as (13) from the estimated back EMF. Even though the same principle is used in above two back EMF estimation methods, the state observer is more robust to operating conditions and parameter variations than the direct calculation because of the consideration of current variation and closed loop form of the observer.

Meanwhile, the concept of an Extended EMF is proposed to simplify the estimation of the back EMF [6]. Most Back EMF estimation based sensorless methods have some approximations to simplify from the complex equations,(4)-(8), to (11). By applying the Extended EMF idea, these approximations are not required. Because of the difference of d-axis inductance and q-axis inductance, the voltage equation in the estimated rotor reference frame is complicated. With this idea, all terms related to the inductance saliency are moved to the new back EMF terms in voltage equations. And, the modified voltage equation in the estimated rotor reference frame would be simple and the sensorless algorithm can be implemented easily and accurately. This modified back EMF term is so called as Extended EMF. The revised voltage equation can be described with Extended EMF, E_{ex} as (16).

$$\begin{aligned} v_{ds}^{r} &= R_s i_{ds}^{r} + L_{ds}\frac{di_{ds}^{r}}{dt} - \omega_r L_{qs} i_{qs}^{r} \\ v_{qs}^{r} &= R_s i_{qs}^{r} + L_{ds}\frac{di_{qs}^{r}}{dt} + \omega_r L_{qs} i_{ds}^{r} + E_{ex} \\ E_{ex} &= \omega_r\left[\left(L_{ds} - L_{qs}\right) i_{ds}^{r} + \lambda_f\right] - \left(L_{ds} - L_{qs}\right)\frac{di_{qs}^{r}}{dt} \end{aligned} \quad . \tag{16}$$

The voltage equation should be transformed to the estimated rotor reference frame by position error, $\tilde{\theta}_r$. Then, the voltage equation in (16) can be described as (17) in the estimated rotor reference frame.

$$\begin{aligned} v_{ds}^{\hat{r}} &= R_s i_{ds}^{\hat{r}} + L_{ds}\frac{di_{ds}^{\hat{r}}}{dt} - \omega_r L_{qs} i_{qs}^{\hat{r}} + e_{ds}^{\hat{r}} \\ v_{qs}^{\hat{r}} &= R_s i_{qs}^{\hat{r}} + L_{ds}\frac{di_{qs}^{\hat{r}}}{dt} + \omega_r L_{qs} i_{ds}^{\hat{r}} + e_{qs}^{\hat{r}} \end{aligned} \tag{17}$$

$$\text{where } \begin{bmatrix} e_{ds}^{\hat{r}} \\ e_{qs}^{\hat{r}} \end{bmatrix} = E_{ex}\begin{bmatrix} -\sin\tilde{\theta}_r \\ \cos\tilde{\theta}_r \end{bmatrix} + \left(\hat{\omega}_r - \omega_r\right) L_{ds}\begin{bmatrix} -i_{qs}^{\hat{r}} \\ i_{ds}^{\hat{r}} \end{bmatrix} . \tag{18}$$

From (17) and (18), the state equations can be derived as (19) under the assumption that the derivative of Extended EMF is zero.

$$\begin{aligned} \frac{d}{dt}\begin{bmatrix} \hat{i}_{ds}^{\hat{r}} \\ \hat{e}_{ds}^{\hat{r}} \end{bmatrix} &= \begin{bmatrix} -R_s/L_{ds} & -1/L_{ds} \\ 0 & 0 \end{bmatrix}\begin{bmatrix} \hat{i}_{ds}^{\hat{r}} \\ \hat{e}_{ds}^{\hat{r}} \end{bmatrix} + \begin{bmatrix} 1/L_{ds} \\ 0 \end{bmatrix}\hat{v}_{dsf}^{\hat{r}} \\ \frac{d}{dt}\begin{bmatrix} \hat{i}_{qs}^{\hat{r}} \\ \hat{e}_{qs}^{\hat{r}} \end{bmatrix} &= \begin{bmatrix} -R_s/L_{ds} & -1/L_{ds} \\ 0 & 0 \end{bmatrix}\begin{bmatrix} \hat{i}_{qs}^{\hat{r}} \\ \hat{e}_{qs}^{\hat{r}} \end{bmatrix} + \begin{bmatrix} 1/L_{ds} \\ 0 \end{bmatrix}\hat{v}_{qsf}^{\hat{r}} \end{aligned} \tag{19}$$

$$\text{where } \begin{bmatrix} \hat{v}_{dsf}^{\hat{r}} \\ \hat{v}_{qsf}^{\hat{r}} \end{bmatrix} = \begin{bmatrix} v_{ds}^{\hat{r}} \\ v_{qs}^{\hat{r}} \end{bmatrix} + \omega_r L_{qs}\begin{bmatrix} i_{qs}^{\hat{r}} \\ -i_{ds}^{\hat{r}} \end{bmatrix} . \tag{20}$$

The d-axis and q-axis current and Extended EMF can be estimated separately as (21).

$$\begin{aligned} \frac{d}{dt}\begin{bmatrix} \hat{i}_{ds}^{\hat{r}} \\ \hat{e}_{ds}^{\hat{r}} \end{bmatrix} &= \begin{bmatrix} -R_s/L_{ds} & -1/L_{ds} \\ 0 & 0 \end{bmatrix}\begin{bmatrix} \hat{i}_{ds}^{\hat{r}} \\ \hat{e}_{ds}^{\hat{r}} \end{bmatrix} + \begin{bmatrix} 1/L_{ds} \\ 0 \end{bmatrix} v_{dsf}^{\hat{r}} + \begin{bmatrix} l_1 \\ l_2 \end{bmatrix}\left(i_{ds}^{\hat{r}} - \begin{bmatrix} 1 & 0 \end{bmatrix}\begin{bmatrix} \hat{i}_{ds}^{\hat{r}} \\ \hat{e}_{ds}^{\hat{r}} \end{bmatrix}\right) \\ \frac{d}{dt}\begin{bmatrix} \hat{i}_{qs}^{\hat{r}} \\ \hat{e}_{qs}^{\hat{r}} \end{bmatrix} &= \begin{bmatrix} -R_s/L_{ds} & -1/L_{ds} \\ 0 & 0 \end{bmatrix}\begin{bmatrix} \hat{i}_{qs}^{\hat{r}} \\ \hat{e}_{qs}^{\hat{r}} \end{bmatrix} + \begin{bmatrix} 1/L_{ds} \\ 0 \end{bmatrix} v_{qsf}^{\hat{r}} + \begin{bmatrix} l_1 \\ l_2 \end{bmatrix}\left(i_{qs}^{\hat{r}} - \begin{bmatrix} 1 & 0 \end{bmatrix}\begin{bmatrix} \hat{i}_{qs}^{\hat{r}} \\ \hat{e}_{qs}^{\hat{r}} \end{bmatrix}\right) \end{aligned} \tag{21}$$

Under the assumption that the speed error is small, the Extended EMF can be simplified as (22). From the estimated Extended EMF, the position error is derived as (23).

$$\begin{bmatrix} \hat{e}_{ds}^{\hat{r}} \\ \hat{e}_{qs}^{\hat{r}} \end{bmatrix} = E_{ex}\begin{bmatrix} -\sin\tilde{\theta}_r \\ \cos\tilde{\theta}_r \end{bmatrix} . \tag{22}$$

$$\tilde{\theta}_r = \tan^{-1}\left(\frac{-\hat{e}_{ds}^{\hat{r}}}{\hat{e}_{qs}^{\hat{r}}}\right) . \tag{23}$$

The state observer with the extended EMF in this method is simpler than that in the previous back EMF estimation method, and d-axis and q-axis state are estimated separately.

C. *Voltage/Current Model Sensorless Methods*

As another approach based on back EMF, the difference between the estimated voltage/current and the actual voltage/current can be used to extract the position error [7]. Key idea of this approach is following:

a) If the model of AC machine is exact with the actual machine, the voltage and/or current can be calculated exactly.
b) If there are differences between the actual voltage and/or current and the calculated ones based on the model, the difference may come from the position error between the actual position and the estimated position.
c) From the differences, the position error can be estimated.

From the voltage model, the voltage can be derived as (24) under the assumption that position error is zero.

$$\begin{aligned} v_{dsM}^{\hat{r}} &= R_s i_{ds}^{\hat{r}} + L_{ds}\frac{di_{ds}^{\hat{r}}}{dt} - \omega_r L_{qs} i_{qs}^{\hat{r}} \\ v_{qsM}^{\hat{r}} &= R_s i_{qs}^{\hat{r}} + L_{ds}\frac{di_{qs}^{\hat{r}}}{dt} + \omega_r L_{qs} i_{ds}^{\hat{r}} + \omega_r \lambda_f \end{aligned} \quad . \tag{24}$$

From (24), the rotating speed can be directly calculated as (25). Then, the d-axis voltage can be described as (26).

$$\hat{\omega}_{rCal} = \frac{v_{qs}^{\hat{r}} - R_s i_{qs}^{\hat{r}} - L_{qs} p i_{qs}^{\hat{r}}}{\lambda_f + L_{ds} i_{ds}^{\hat{r}}} \quad . \tag{25}$$

$$v_{dsM}^{\hat{r}} = R_s i_{ds}^{\hat{r}} + L_{ds}\frac{di_{ds}^{\hat{r}}}{dt} - \hat{\omega}_{rCal} L_{qs} i_{qs}^{\hat{r}} \quad . \tag{26}$$

And, the d-axis voltage difference between (24) and (11) can be obtained as (27).

$$\Delta v_{ds}^{\hat{r}} = v_{ds}^{\hat{r}} - v_{dsM}^{\hat{r}} = -\omega_r \lambda_f \sin\tilde{\theta}_r \quad . \tag{27}$$

The calculated speed, (25) and the position error in (27) can be used for the estimation of speed and position as shown in Fig.4.

In the similar way, the difference between the actual current and the calculated current can be used as a position error. The current equation can be derived from (24) as (28).

$$\begin{aligned} \frac{di_{dsM}^{\hat{r}}}{dt} &= \frac{1}{L_{ds}}\left\{v_{ds}^{\hat{r}} - R_s i_{ds}^{\hat{r}} + \hat{\omega}_r L_{qs} i_{qs}^{\hat{r}}\right\} \\ \frac{di_{qsM}^{\hat{r}}}{dt} &= \frac{1}{L_{qs}}\left\{v_{qs}^{\hat{r}} - R_s i_{qs}^{\hat{r}} - \hat{\omega}_r L_{ds} i_{ds}^{\hat{r}} - \hat{\omega}_r \lambda_f\right\} \end{aligned} \quad . \tag{28}$$

However, the actual motor currents are affected by the position error. Therefore, the actual current can be derived from (11), considering the position error.

$$\begin{aligned} \frac{di_{ds}^{\hat{r}}}{dt} &= \frac{1}{L_{ds}}\left\{v_{ds}^{\hat{r}} - R_s i_{ds}^{\hat{r}} + \omega_r L_{qs} i_{qs}^{\hat{r}} + \omega_r \lambda_f \sin\tilde{\theta}_r\right\} \\ \frac{di_{qs}^{\hat{r}}}{dt} &= \frac{1}{L_{qs}}\left\{v_{qs}^{\hat{r}} - R_s i_{qs}^{\hat{r}} - \omega_r L_{ds} i_{ds}^{\hat{r}} - \omega_r \lambda_f \cos\tilde{\theta}_r\right\} \end{aligned} \quad . \tag{29}$$

The difference between the current from (28) and from (29) can also reveal the position and speed error as (30).

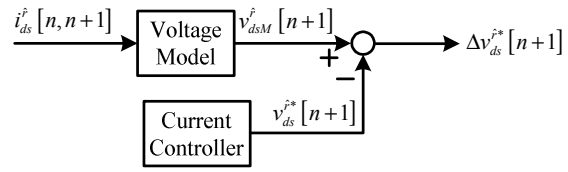

(a) Voltage model and voltage error

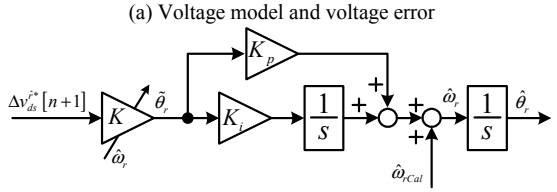

(b) Speed and position estimation

Fig. 4. Block diagram of voltage model based sensorless method

$$\begin{bmatrix}\Delta i_{ds}^{\hat{r}}\\ \Delta i_{qs}^{\hat{r}}\end{bmatrix}=\begin{bmatrix} i_{ds}^{\hat{r}}-i_{dsM}^{\hat{r}}\\ i_{qs}^{\hat{r}}-i_{qsM}^{\hat{r}}\end{bmatrix}=\lambda_f T_s\begin{bmatrix}\omega_r\sin\tilde{\theta}_r \big/ L_{ds}\\ -\omega_r\cos\tilde{\theta}_r+\hat{\omega}_r \big/ L_{qs}\end{bmatrix}\approx\lambda_f T_s\begin{bmatrix}\omega_r\tilde{\theta}_r \big/ L_{ds}\\ -\tilde{\omega}_r \big/ L_{qs}\end{bmatrix} \quad (30)$$

where T_S is a sampling period of the sensorless controller.

From (30), the q-axis current difference can be used to estimate the rotating speed because that is related to the speed error between the actual speed and the estimated speed. And the d-axis current difference has information regarding position error. Therefore the speed and position estimation can be implemented as Fig. 5.

D. Fundamental Voltage Feedback Sensorless Methods

Unlike the back EMF estimation or model based methods, the voltage reference of the current controller can be directly used as the position error related values [8]. The difference between the voltage equation considering the position error, (11), and the ideal voltage equation under the assumption of no position error (1), reveals the position error. If the motor parameter is known exactly and the feed-forwarding voltage in the current controller is defined as (31), the d-axis output voltage of P-I controller should be zero in electrically steady state. However, if there is position error, the d-axis voltage reference would be affected by the position error as (32).

$$\begin{aligned} v_{dsff}^{\hat{r}} &= R_s i_{ds}^{\hat{r}}-\omega_r L_{qs} i_{qs}^{\hat{r}}\\ v_{qsff}^{\hat{r}} &= R_s i_{qs}^{\hat{r}}+\omega_r L_{ds} i_{ds}^{\hat{r}}+\omega_r\lambda_f \end{aligned} \quad (31)$$

$$v_{dsfb}^{\hat{r}}=v_{ds}^{\hat{r}}-v_{dsff}^{\hat{r}}\approx-\omega_r\lambda_f\sin\tilde{\theta}_r \quad . \quad (32)$$

Neglecting the electric transient, the d-axis voltage output of P-I controller includes information regarding the position error. In Fig. 6, the d-axis voltage difference in (32) is used as an input to a PI type compensator to nullify the rotor position error. Even though the implementation is very simple and easy, the machine parameter variations are not considered, and because of the assumption of the steady state the current transient causes the deterioration of position estimation performance.

III. SALIENCY BASED SENSORLESS CONTROL

A. Fundamental Principle

At the standstill or very low rotating speed, the rotor position can be estimated by using the magnetic saliency of machine: the spatial inductance distribution is determined by the rotor position because of the saliency of the magnetic path. The magnetic saliency can be expressed in the stationary reference voltage equation as (33).

$$\begin{bmatrix}v_{ds}^{s}\\ v_{qs}^{s}\end{bmatrix}=R_s\begin{bmatrix}i_{ds}^{s}\\ i_{qs}^{s}\end{bmatrix}+\frac{d}{dt}\begin{bmatrix}\lambda_{ds}^{s}\\ \lambda_{qs}^{s}\end{bmatrix} \quad (33)$$

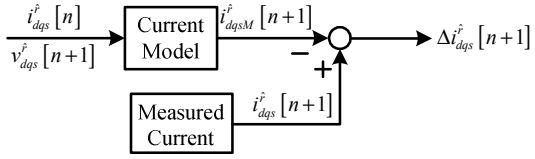

(a) Current model and current error

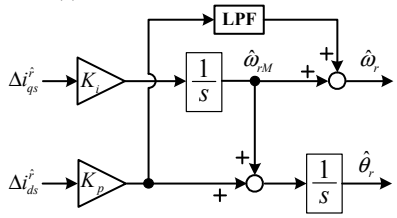

(b) Speed and position estimation

Fig. 5. Block diagram of current model based sensorless method

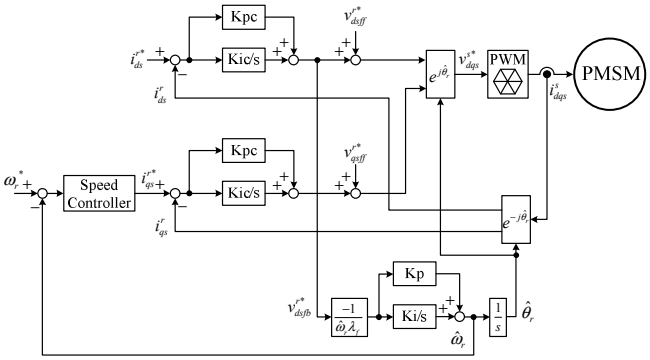

Fig. 6. Block diagram of voltage feedback sensorless method

where $[v_{ds}^{s}, v_{qs}^{s}]^{\mathrm{T}}$, $[i_{ds}^{s}, i_{qs}^{s}]^{\mathrm{T}}$, and $[\lambda_{ds}^{s}, \lambda_{qs}^{s}]^{\mathrm{T}}$ are the vectors of the stator voltage, current, and flux linkage in the stationary d-q-axis reference frame, respectively. Physically, the flux linkage in stationary reference frame in (33), $[\lambda_{ds}^{s}, \lambda_{qs}^{s}]^{\mathrm{T}}$, are function of the stator currents, and the flux linkage of the permanent magnet on the rotor. Those flux linkages can be derived as (34).

$$\begin{bmatrix}\lambda_{ds}^{s}\\ \lambda_{qs}^{s}\end{bmatrix}=L_S\begin{bmatrix}i_{ds}^{s}\\ i_{qs}^{s}\end{bmatrix}+\lambda_f\begin{bmatrix}\cos\theta_r\\ \sin\theta_r\end{bmatrix} \quad . \quad (34)$$

The inductance matrix, L_s, can be derived with d-q-axis inductance in the rotor reference frame and the rotor position, θ_r, as (35).

$$L_S=\begin{bmatrix}\Sigma L+\Delta L\cos 2\theta_r & \Delta L\sin 2\theta_r\\ \Delta L\sin 2\theta_r & \Sigma L-\Delta L\cos 2\theta_r\end{bmatrix}$$
$$\text{where } \Sigma L=\frac{L_{ds}+L_{qs}}{2} \quad \Delta L=\frac{L_{ds}-L_{qs}}{2} \quad . \quad (35)$$

Then, the voltage equation can be rewritten by substituting the flux linkage with inductances and the stator currents as (36).

$$\begin{aligned}\begin{bmatrix}v_{ds}^{s}\\ v_{qs}^{s}\end{bmatrix}&=R_s\begin{bmatrix}i_{ds}^{s}\\ i_{qs}^{s}\end{bmatrix}+\begin{bmatrix}\Sigma L+\Delta L\cos 2\theta_r & \Delta L\sin 2\theta_r\\ \Delta L\sin 2\theta_r & \Sigma L-\Delta L\cos 2\theta_r\end{bmatrix}\frac{d}{dt}\begin{bmatrix}i_{ds}^{s}\\ i_{qs}^{s}\end{bmatrix}\\ &+\omega_r\left(2\Delta L\begin{bmatrix}-\sin 2\theta_r & \cos 2\theta_r\\ \cos 2\theta_r & \sin 2\theta_r\end{bmatrix}\begin{bmatrix}i_{ds}^{s}\\ i_{qs}^{s}\end{bmatrix}+\lambda_f\begin{bmatrix}-\sin\theta_r\\ \cos\theta_r\end{bmatrix}\right)\end{aligned} \quad (36)$$

In (36), it can be seen that the position information is included in two components: inductances in the second term and fundamental flux in the third term of right side of (36). Because the rotating speed, ω_r is zero or very small at standstill or low speed, the magnitude of the third term is very small compared to other terms. And, the third term cannot be used for the position estimation. Hence, the second term can be used for the estimation of the rotor position.

To extract the spatial inductance variation in the third term of (36), the relationship between current and voltage should be employed. To examine this current-voltage relationship, the high

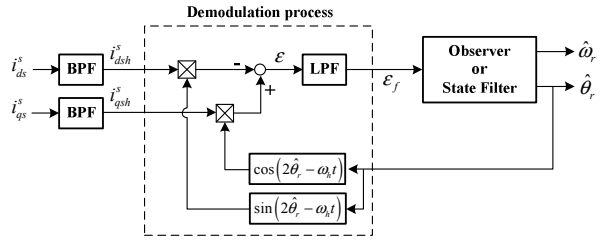

Fig. 7. Block diagram of the heterodyning demodulation process in the rotating voltage vector injection method in the stationary reference frame.

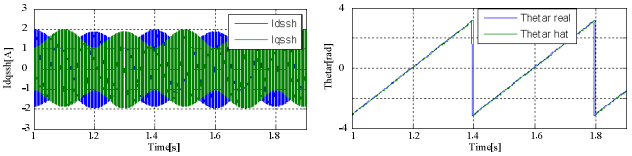

(a) High frequency current response (b) Rotor position estimation result

Fig. 8. Simulation results of the rotating voltage signal injection sensorless method.

frequency voltage signal injection methods are generally adopted. Supposing the high frequency voltage signal is injected into the machine, the high frequency impedance model of IPMSM can be simply derived as (37).

$$\begin{bmatrix} v_{dsh}^s \\ v_{qsh}^s \end{bmatrix} = \begin{bmatrix} \Sigma L + \Delta L\cos 2\theta_r & \Delta L\sin 2\theta_r \\ \Delta L\sin 2\theta_r & \Sigma L - \Delta L\cos 2\theta_r \end{bmatrix} \frac{d}{dt}\begin{bmatrix} i_{dsh}^s \\ i_{qsh}^s \end{bmatrix} \quad . \quad (37)$$

To extract the position information from (37), the various type voltage signals can be injected into the machine, and the many demodulation processes had been proposed according to the injected signal type.

B. Rotating Voltage Signal Injection in Stationary Frame

If voltage signal in (38) is injected to the stationary reference frame, the locus of the injected voltage vector would be a circle [9].

$$\begin{bmatrix} v_{dsh}^s \\ v_{qsh}^s \end{bmatrix} = V_{inj}\begin{bmatrix} -\sin\omega_h t \\ \cos\omega_h t \end{bmatrix} \quad (38)$$

where V_{inj} and ω_h are the amplitude and frequency of the injection signal, respectively. According to this rotating voltage signal, the corresponding current response from (37) can be derived as (39).

$$\begin{bmatrix} i_{dsh}^s \\ i_{qsh}^s \end{bmatrix} = \frac{V_{inj}}{\Sigma L^2 - \Delta L^2}\begin{bmatrix} \frac{\Sigma L}{\omega_h}\cos\omega_h t + \frac{\Delta L}{2\omega_r - \omega_h}\cos(2\theta_r - \omega_h t) \\ \frac{\Sigma L}{\omega_h}\sin\omega_h t + \frac{\Delta L}{2\omega_r - \omega_h}\sin(2\theta_r - \omega_h t) \end{bmatrix} \quad . \quad (39)$$

From the current response, (39), the position information can be extracted through a kind of signal processing so called as demodulation process. In Fig. 7 a heterodyning demodulation process is shown. Before the demodulation process, the injected high frequency component from the measured phase current are extracted through a Band-Pass-Filter (BPF). Then, the high frequency components are multiplied with sinusoidal function whose frequency is identical to the injection frequency. After low-pass-filtering, the final result of the demodulation process, ε_f in Fig. 7, can be derived as (40) under the assumption that ω_h, is large enough compared to the rotating speed, ω_r, ($\omega_h >> \omega_r$) and that the rotor position error is reasonably small.

$$\varepsilon_f \approx \frac{-V_{inj}}{\Sigma L^2 - \Delta L^2}\frac{\Delta L}{\omega_h} 2\left(\theta_r - \hat{\theta}_r\right) = K\tilde{\theta}_r \quad . \quad (40)$$

Applying an observer or a state filter after the demodulation process, the rotor position and speed can be estimated. In Fig. 8, a typical current response according to the rotating voltage injection and the estimated position through the signal processing mentioned above are shown by the computer simulation.

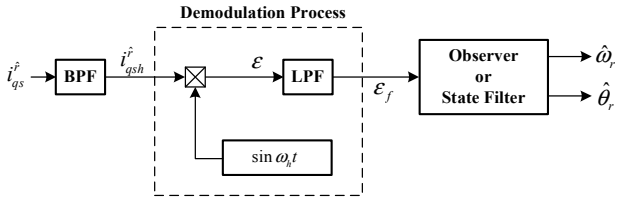

Fig. 9. Block diagram of the heterodyning demodulation process.

C. Pulsating Voltage Signal Injection in Estimated Rotor Reference Frame

Similarly, the rotor position can be estimated by the pulsating signal injection in the estimated rotor reference frame [10]. The voltage equation in the exact rotor reference frame can be described as (1). With the high frequency voltage signal injection into IPMSM, the high frequency impedance model in the rotor reference frame can be described as (41).

$$\begin{bmatrix} v_{dsh}^r \\ v_{qsh}^r \end{bmatrix} = \begin{bmatrix} L_{ds} & 0 \\ 0 & L_{qs} \end{bmatrix} \frac{d}{dt}\begin{bmatrix} i_{dsh}^r \\ i_{qsh}^r \end{bmatrix} \quad . \quad (41)$$

When the pulsating voltage signal is injected into d-axis at the rotor reference frame, the corresponding current response includes the rotor position information. However, the voltage as (42) is not injected on the actual rotor reference frame but on the estimated rotor reference frame. Then the actual injected voltage in the actual rotor reference frame can be deduced as (43).

$$\begin{bmatrix} v_{dsh}^{\hat{r}} \\ v_{qsh}^{\hat{r}} \end{bmatrix} = V_{inj}\begin{bmatrix} \cos\omega_h t \\ 0 \end{bmatrix} \quad (42)$$

$$\begin{bmatrix} v_{dsh}^r \\ v_{qsh}^r \end{bmatrix} = T_{\tilde{\theta}_r}\begin{bmatrix} v_{dsh}^{\hat{r}} \\ v_{qsh}^{\hat{r}} \end{bmatrix} = V_{inj}\begin{bmatrix} \cos\tilde{\theta}_r\cos\omega_h t \\ -\sin\tilde{\theta}_r\cos\omega_h t \end{bmatrix} \quad (43)$$

Then, the current response according to the injected voltage signal can be derived as (44) from (41) and (43).

$$\begin{bmatrix} i_{dsh}^{\hat{r}} \\ i_{qsh}^{\hat{r}} \end{bmatrix} = T_{\tilde{\theta}_r}^{-1}\begin{bmatrix} i_{dsh}^r \\ i_{qsh}^r \end{bmatrix} = \frac{V_{inj}}{\omega_h}\begin{bmatrix} \left(\frac{\cos^2\omega_h t}{L_{ds}} + \frac{\sin^2\omega_h t}{L_{qs}}\right)\sin\omega_h t \\ \frac{1}{2}\left(\frac{-\Delta L}{L_{ds}L_{qs}}\right)\sin 2\tilde{\theta}_r\sin\omega_h t \end{bmatrix} \quad (44)$$

It can be seen from (44), the rotor position error is included in the q-axis current response. To extract the rotor position error, various demodulation processes had been proposed. In Fig. 9, a heterodyning demodulation process using the q-axis current response only is shown. The result of this demodulation process can be presented as (45).

$$\varepsilon_f \approx \frac{1}{2}\frac{V_{inj}}{\omega_h}\left(\frac{-\Delta L}{L_{ds}L_{qs}}\right)\left(\theta_r - \hat{\theta}_r\right) = K\tilde{\theta}_r \quad . \quad (45)$$

Like the case of the rotating signal injection method, the result can be used as a corrective error input to an observer or a state filter. In the other hand, using the 45° shifted reference frame in Fig. 10, the rotor position error can be extracted. With this method, the position error can be obtained by difference between magnitudes of currents in d_m-q_m axis.

In Fig. 11, a typical current response according to the pulsating voltage injection and the estimated rotor position are shown by the computer simulation.

D. High Frequency Signal Injection Methods

Though the signal injection sensorless methods can detect the rotor position in any operating condition, there are still several issues: the acoustic noises, additional losses associated with the injected signal, voltage margin to inject high frequency signal, and the limited control bandwidth due the delay in the signal

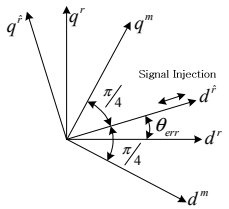

Fig. 10 Real, estimated and measurement axis in the rotor reference frame.

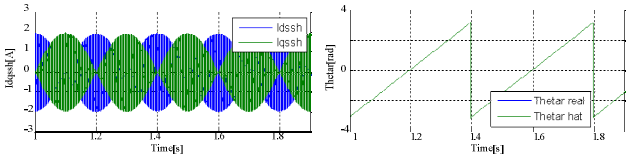

(a) High frequency current response (b) Rotor position estimation result

Fig. 11 Simulation results of the pulsating voltage signal injection sensorless method.

processing. The injection frequency is, usually, from several hundreds Hz to a few kHz. These frequency ranges are in the audible ranges, and it may be offensive to humans. One way to solve this issue would be increasing the injection frequency to around 20kHz, which is out of audible range. Then, the switching frequency of PWM inverter would be much higher than that of the general purpose inverter, and the switching loss would be prohibitive.

The higher frequency signal injection increases the losses associated the injected signal. Though the rms magnitude of the current at the injected frequency is quite small, non negligible copper loss may occur due to the skin effect of the stator winding. Also, the core loss would increases due to the higher frequency current and fluxes flowing through the magnet and cores.

To inject the signal at higher frequency, the voltage margin of PWM inverter should be secured. In a few kW range IPMSM drive, to inject a few kHz signal injection, several tens percents of the rated voltage of the inverter should be devoted to get a reasonable magnitude of the high frequency component current for enough signal to noise ratio in the signal processing.

The bandwidth of torque control and that of other outer control loop such as speed and position loop are limited due the limited bandwidth of the rotor position identification loop. If the frequency of injected voltage is getting higher, the bandwidth can be higher. But the cost for the higher frequency signal injection is evident as mentioned above. Hence, in sensorless drive, still there are many research topics to solve to lessen above issues. In the last couple years, there are several achievements in these issues. The performance of the sensorless drive has been remarkably enhanced and it is comparable to that of the low end sensored servo drive.

In [11] [12], the signal injection whose frequency is a half of the PWM switching, are implemented with the conventional SVPWM. In this case, the number of the sampling of the current values are four times only in an injection signal period. Because of the small number of current sampling, it is hard to extract the rotor position exactly with the conventional heterodyning demodulation processes. Therefore, the magnitude of the current ripple itself is used as the position corrective value. And the demodulation process is circumvented. And, the bandwidth of the speed control loop has been increased up to 50 Hz, that is almost one order higher than the bandwidth of the sensorless drive based on heterodyning process. In [13], the two third of PWM frequency signal injection method is implemented and it is proposed that the position is directly calculated with voltage and current differences only. If the PWM switching frequency increases above 20 kHz, which is the possible switching frequency with up to date IGBT technology, the acoustic noise problem with this method would be diminished to virtually null.

IV. Conclusion

Position sensorless control of AC machine is attractive technology that can reduce system cost and increase the robustness and reliability of the entire drive system. In overall rotating speed region except zero and low speed operation, the back EMF based sensorless methods have been prevailed. The performances of those methods are acceptable, and the sensorless drives have been used widely from industrial applications to home appliances for last two decades. For the jump of the performance of the sensorless drive, the signal injection sensorless methods have attracted many attentions. In some industrial application such as elevator drive system and oil pump motor drive, the initial position of the IPMSM have been detected with the high frequency signal injection methods for last 5 years. Still, acoustic noise was a burden for wide acceptance of the high frequency signal injection method.

However, since year 2008, there has been a product to drive general purpose IPMSM employing high frequency signal injection method. The product is successfully deployed in many industrial applications such as a lift, a compressor, and an injection molding machine [14],[15]. Now, the sensorless drives using high frequency signal injection together with specially designed IPMSM are under evaluation for hybrid/electric vehicle traction. Regardless of these recent achievements, still there are many issues and topics for the improvement of the performance of the sensorless drive. In near future, we can see the position sensor of IPMSM be obsolete.

References

[1] D. W. Novotny, and T. A. Lipo, "Vector control and dynamics of AC drives," Clarendon Press, Oxford, 1996.

[2] J. Holtz, "Sensorless control of induction machines- with or without signal injection?," *IEEE Trans. Ind. Electron.*, vol. 53, no. 1, pp. 7-30, Feb. 2006.

[3] P. P. Acarnley, and J. F. Watson, "Review of position-sensorless operation of brushless permanent-magnet machines," *IEEE Trans. Ind. Electron.*, vol. 53, no. 2, pp. 352-362, Apr. 2006.

[4] Yaskawa America, Inc.: Industrial AC drives A1000 manual, "http://www.yaskawa.com/site/products.nsf/products/Industrial%20AC%20Drives~A1000.html"

[5] Y.-C. Son, B.-H Bae, and S.-K Sul, "Sensorless operation of permanent magnet motor using direct voltage sensing circuit," in *Proc. IEEE IAS*, 2002, pp. 1674-1678.

[6] S. Morimoto, K. Kawamoto, M. Sanada, and Y. Takeda, "Sensorless control strategy for salient-pole PMSM based on extended EMF in rotating reference frame," *IEEE Trans. Ind. Appl.*, vol. 38, no. 4, pp. 1054-1061, Jul./Aug. 2002.

[7] N. Matsui, "Sensorless operation of brushless DC motor drives," in *Proc. IEEE IECON'93*, 1993, pp. 739-744.

[8] B.-H. Bae, S.-K. Sul, J.-H. Kwon, and J.-S. Byeon, "Implementation of sensorless vector control for super-high-speed PMSM of turbo-compressor," *IEEE Trans. Ind. Appl.*, vol. 39, no. 3, pp. 811-818, May/Jun. 2003.

[9] P. L. Jansen, and R. D. Lorenz, "Transducerless position and velocity estimation in induction and salient AC machines," *IEEE Trans. Ind. Appl.*, vol. 31, no. 2, pp. 240-247, Mar./Apr. 1995.

[10] J.-I. Ha, and S.-K. Sul, "Sensorless field-orientation control of an induction machine by high-frequency signal injection," *IEEE Trans. Ind. Appl.*, vol. 35, no. 1, pp. 45-51, Jan./Feb. 1999.

[11] Y.-D. Yoon, S.-K. Sul, S. Morimoto, and K. Ide, "High bandwidth sensorless algorithm for AC machines based on square-wave-type voltage injection," *IEEE Trans. Ind. Appl.*, vol. 47, no. 3, pp. 1361-1370, May/Jun. 2011.

[12] R. Leidhold, and P. Mutschler, "Improved method for higher dynamics in sensorless position detection," in Proc. *IEEE IECON2008*, 2008, pp. 1240-1245..

[13] S. Kim, Y.-C. Kwon, S.-K. Sul, J. Park, and S.-M. Kim, "Position sensorless operation of IPMSM with near PWM switching frequency signal injection," in *Proc. ICPE2011-ECCE Asia*, 2011, pp. 1660-1665.

[14] S. Sato, H. Iura, K. Ide, and S-.K. Sul, "Three years of industrial experience with sensorless IPMSM drive based on high frequency injection method," to be appeared in *Pro., Symposium on sensorless control for electrical drives(SLED), 2011.*

[15] K. Ide, M. Hisatsune, T. Shiota, S. Murakami, and M. Ohto, "Encoderless servo drive with adequately designed IPMSM for saliency-based position detection, " in *Proc. ICPE2011-ECCE Asia*, 2011, pp. 1257-1264.